

# Hierarchically Ordered Structures Enabled by Controlled Evaporative Self-Assembly

Myunghwan Byun, Wei Han, Feng Qiu, Ned B. Bowden, and Zhiqun Lin\*

Hierarchical structures are common in both nature and technology. In the latter context, controlling the spatial arrangement of components over multiple length scales (i.e., forming hierarchically ordered structures) is highly desirable for many applications, such as lab-on-a-chip devices, integrated circuits, and microelectromechanical systems (MEMSs).<sup>[1]</sup> Most hierarchically ordered structures are fabricated by very costly, complicated, and destructive surface patterning techniques that rely heavily on lithographic conditions (e.g., electron-beam (e-beam) or deep-UV), the use of additional external forces (e.g., electric or magnetic fields), and the use of sophisticated multistep processing. By contrast, a simple yet promising strategy to create complex, hierarchically ordered structures is the combination of top-down controlled evaporative self-assembly with bottom-up molecular self-assembly.

Evaporative self-assembly of nonvolatile solutes (e.g., polymers, viruses, DNA, latex particles, nanocrystals, and carbon nanotubes) from a sessile droplet yields a rich family of intriguing structures<sup>[2–4]</sup> possessing submicrometer dimensions and larger. These structures, however, often lack regularity. In order to take advantage of the extreme simplicity of this top-down technique and to exploit its full potential in many applications, control of the evaporative flux, solution concentration, and interfacial interactions of the solvent, solute, and substrate is necessary to produce highly ordered, complex structures. In a number of studies that elegantly demonstrated precise control over droplet evaporation,<sup>[5–15]</sup> including the controlled anisotropic wetting/

dewetting processes<sup>[13,14]</sup> and convective assembly in evaporating menisci,<sup>[15]</sup> controlled evaporative self-assembly in a restricted geometry has been shown to create complex deposit patterns with unprecedented regularity.<sup>[16–19]</sup> Diblock copolymers composed of two chemically dissimilar chains joined together at one end spontaneously self-assemble into a range of well-ordered, microphase-separated nanoscopic structures including spheres, cylinders, gyroids, and lamellae, depending on the volume fractions of the blocks, with sizes on the scale of 10 to 100 nm. Diblock copolymers are widely recognized as attractive building blocks for bottom-up nanofabrication processes, offering an areal density of  $10^{13}$  nanostructures per square inch for potential use in photonics, nanoelectronics, magnetic data storage, nanotechnology, and biotechnology.<sup>[20–23]</sup>

Here, we report a simple yet robust technique to achieve hierarchically ordered structures by combining two self-assembly processes on different length scales, namely, top-down controlled evaporative self-assembly with bottom-up spontaneous self-assembly of nanomaterials, i.e., comb block copolymer (CBCP). Highly ordered, microscopic concentric CBCP rectangles in a gradient arrangement are formed via evaporative self-assembly, as a result of controlled pinning and depinning of a three-phase contact line of evaporating CBCP toluene solution confined in a wedge-on-flat geometry. Subsequent solvent vapor annealing promoted spontaneous microphase separation of CBCP, thereby leading to the formation of nanocylinders oriented vertically to the surface of thin stripes. These hierarchically ordered structures may offer new opportunities for use in optics, electronics, optoelectronic materials, and miniaturized devices and serve as a useful platform to study cell motility and adhesion and neuron guidance.

A newly synthesized amphiphilic, asymmetric CBCP with an ultrahigh molecular weight ( $MW = 510 \text{ kg mol}^{-1}$ ; degree of polymerization along the backbone exceeding 1100 units) was used as a nonvolatile solute (**Figure 1a**).<sup>[24,25]</sup> The block with the polystyrene arms (i.e., the C block) possesses a rigid rod shape due to the steric crowding between the arms, resulting in elongation of the backbone polymer in that block (**Figure 1b**).<sup>[26]</sup> CBCPs can be readily assembled into ordered morphologies (i.e., cylindrical nanodomains) because the size of the backbone polymer is analogous to that of linear block copolymers.<sup>[24,25]</sup> The large domain size, close to 100 nm, and well-defined molecular structure of CBCP make it an excellent candidate to study the microphase-separated structures,<sup>[26]</sup> as well as the confinement effect on the ordering of nanocylinders within thin CBCP stripes produced via simple

---

M. Byun, W. Han, Prof. Z. Lin  
Department of Materials Science and Engineering  
Iowa State University  
Ames, IA 50011, USA  
E-mail: zqlin@iastate.edu

Prof. F. Qiu, Prof. Z. Lin  
Key Laboratory of Molecular Engineering of Polymers  
Fudan University  
Shanghai, 200433, P. R. China

Prof. F. Qiu  
Department of Macromolecular Science  
Fudan University  
Shanghai, 200433, P. R. China

Prof. N. B. Bowden  
Department of Chemistry  
University of Iowa  
Iowa City, IA 52242, USA

DOI: 10.1002/sml.201000816

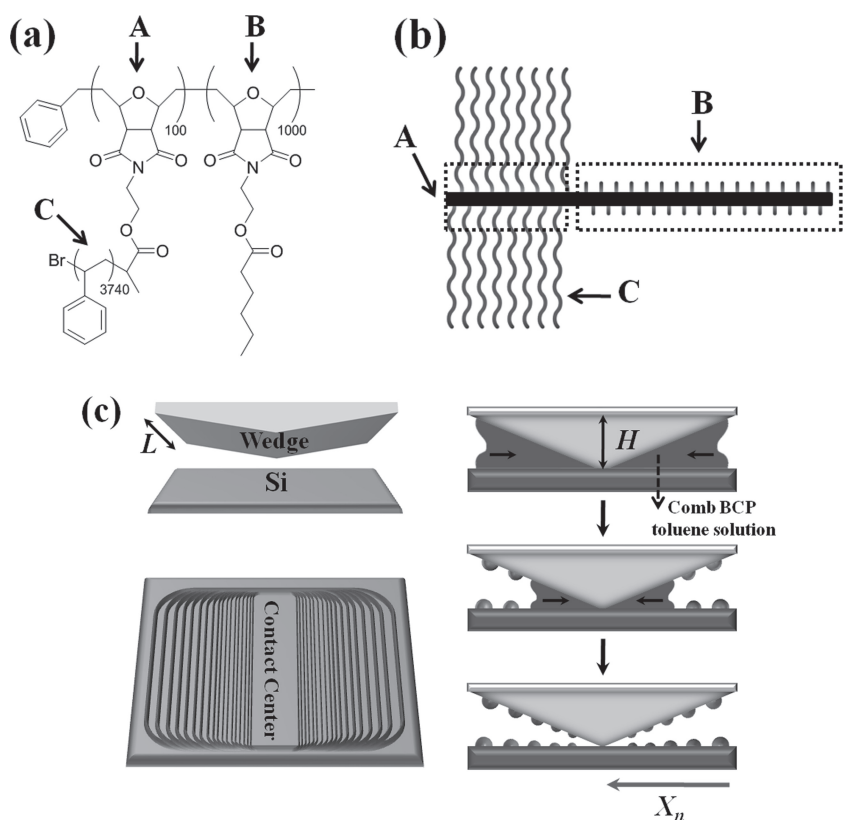


**Figure 1.** a) Chemical structure and b) schematic illustration of newly synthesized CBCP. Each block is labeled as A, B, or C. c) Schematic representation of the route to gradient CBCP stripes. A drop of CBCP toluene solution was trapped in the wedge-on-flat geometry, consisting of a wedge-shaped lens on a flat Si substrate (top left panel), forming a capillary-held solution (side view, top right panel; height,  $H = 1000 \mu\text{m}$ ). As the contact line of the trapped solution retracted toward the wedge/Si contact center by successive controlled “stick-slip” motions, gradient stripes of CBCP over large areas formed (center and bottom right panels; solid lateral arrows mark the movement of the solution front toward the wedge/Si contact center).  $X_n$  indicates the position toward the contact center. Schematic illustration of gradient concentric rectangles deposited globally on the Si substrate (bottom left panel).

evaporative patterning in the wedge-on-flat geometry in the present study.

The CBCP toluene solution was trapped in the gap between a wedge-like lens and a Si substrate, thereby forming a capillary-held microfluid (see Experimental Section). The evaporation rate of toluene was greatest at the capillary edge (right panel in Figure 1c).<sup>[17]</sup> As toluene evaporated, CBCP molecules were transported to the perimeter of the confined CBCP solution to pin the contact line (i.e., the “stick” motion).<sup>[17]</sup> During this deposition process, the initial contact angle of the meniscus at the capillary edge gradually decreased to a critical value due to continuous evaporative loss of toluene, causing the depinning force (i.e., capillary force) to become larger than the pinning force.<sup>[17]</sup> This caused the contact line to retract toward the wedge/Si contact center (i.e., the “slip” motion) and pin at a new position, thereby leaving behind a stripe locally (center right panel in Figure 1c).<sup>[17]</sup> Consecutive controlled “stick-slip” cycles of the receding contact line in the symmetric wedge-on-Si geometry yielded concentric rectangle-like deposits globally, guided by the shape of the wedge, as depicted in lower left panel in Figure 1c.

After the evaporation was complete, the patterns formed on the Si substrate were examined by optical microscopy. **Figure 2** shows a typical optical microscopy image of highly ordered, microscopic CBCP stripes locally formed in the wedge-on-Si geometry (left of the cutting line), where  $X_n$  ( $n$  ranging from 1 to 5) indicates the position away from the wedge/Si contact center (bottom right panel in Figure 1c). The gradient stripes are evident. They appeared more distinctive after tetrahydrofuran (THF) vapor annealing in a sealed vessel for 10 h (to the right of the cutting line in Figure 2; see Experimental Section). It is worth noting that these ordered, self-organized stripes, formed by controlled evaporative assembly of block copolymer solution, were highly reproducible. Compared to concentric rings formed by evaporative self-assembly in a sphere-on-flat geometry,<sup>[17]</sup> the use of a wedge as the upper curved surface yielded straight stripe-like patterns over large areas, which may potentially be integrated into complex microelectronic, optical, and sensing devices.

To further scrutinize the topographic changes of microscopic CBCP stripes and the detailed structural evolution of CBCP nanodomains within the stripes before and after the THF vapor annealing, atomic force microscopy (AFM) measurements were conducted at the same position of the sample,  $X_n$  (i.e., after cutting the as-prepared sample into two pieces, one piece was examined as is, and the other was examined after the vapor treatment). 2D AFM height images of gradient CBCP stripes before and after solvent vapor annealing are shown in **Figure 3**. Locally, they appeared as parallel lines. The distance between adjacent stripes,  $\lambda_{C-C}$ , the height of stripe,  $h$ , and the width of stripe,  $w$ , progressively decreased as the contact line of evaporating solution approached the wedge/Si contact center, from  $\lambda_{C-C} = 4.8 \mu\text{m}$ ,  $w = 3.8 \mu\text{m}$ , and  $h = 22 \text{ nm}$  at  $X_1 = 3100 \mu\text{m}$  (Figure 3a), to  $4.5 \mu\text{m}$ ,  $3.5 \mu\text{m}$ , and  $19 \text{ nm}$  at  $X_2 = 2950 \mu\text{m}$ , to  $4.1 \mu\text{m}$ ,  $3.2 \mu\text{m}$ , and  $17 \text{ nm}$  at  $X_3 = 2800 \mu\text{m}$  (Figure 3b), to  $3.1 \mu\text{m}$ ,  $2.4 \mu\text{m}$ , and  $15 \text{ nm}$  at  $X_4 = 2650 \mu\text{m}$ , to  $2.8 \mu\text{m}$ ,  $2.3 \mu\text{m}$ , and  $12 \text{ nm}$  at  $X_5 = 2500 \mu\text{m}$  (Figure 3c). The gradient dimension of the stripes was a direct consequence of the competition between the linear pinning force and the nonlinear capillary force<sup>[17]</sup> and the decrease in the height of meniscus of the solution due to the tilted surface topology of wedge as the solvent evaporated. Quite intriguingly, after subsequent THF vapor annealing, obvious morphological changes in  $w$  and  $h$  occurred, whereas  $\lambda_{C-C}$  did not vary over the entire sample. The width and height were changed to  $w = 1.8 \mu\text{m}$  and  $h = 44 \text{ nm}$  at  $X_1 = 3100 \mu\text{m}$  (Figure 3d),  $1.6 \mu\text{m}$  and

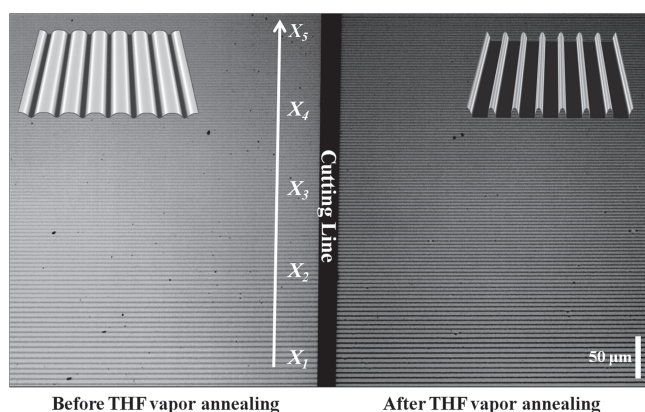


**Figure 2.** Comparison of optical microscopy images of CBCP stripes before and after THF vapor annealing processes from  $X_1$  to  $X_5$ . After evaporative self-assembly of CBCP, the sample was cut into two pieces to allow the examination of morphological changes at the same location of the sample. Compared to as-prepared stripes (left), after THF vapor annealing for 10 h, the visibility of the gradient stripes (right) was greatly improved. An arrow indicates the direction in which the meniscus moved. Scale bar = 50  $\mu\text{m}$ . Two representative 3D AFM height images are shown as insets, signifying the change in stripe dimensions before (left) and after (right) exposure to the solvent vapor.

41 nm at  $X_2 = 2950 \mu\text{m}$ , 1.4  $\mu\text{m}$  and 36 nm at  $X_3 = 2800 \mu\text{m}$  (Figure 3e), 1.3  $\mu\text{m}$  and 34 nm at  $X_4 = 2650 \mu\text{m}$ , and 1.1  $\mu\text{m}$  and 31 nm at  $X_5 = 2500 \mu\text{m}$  (Figure 3f).

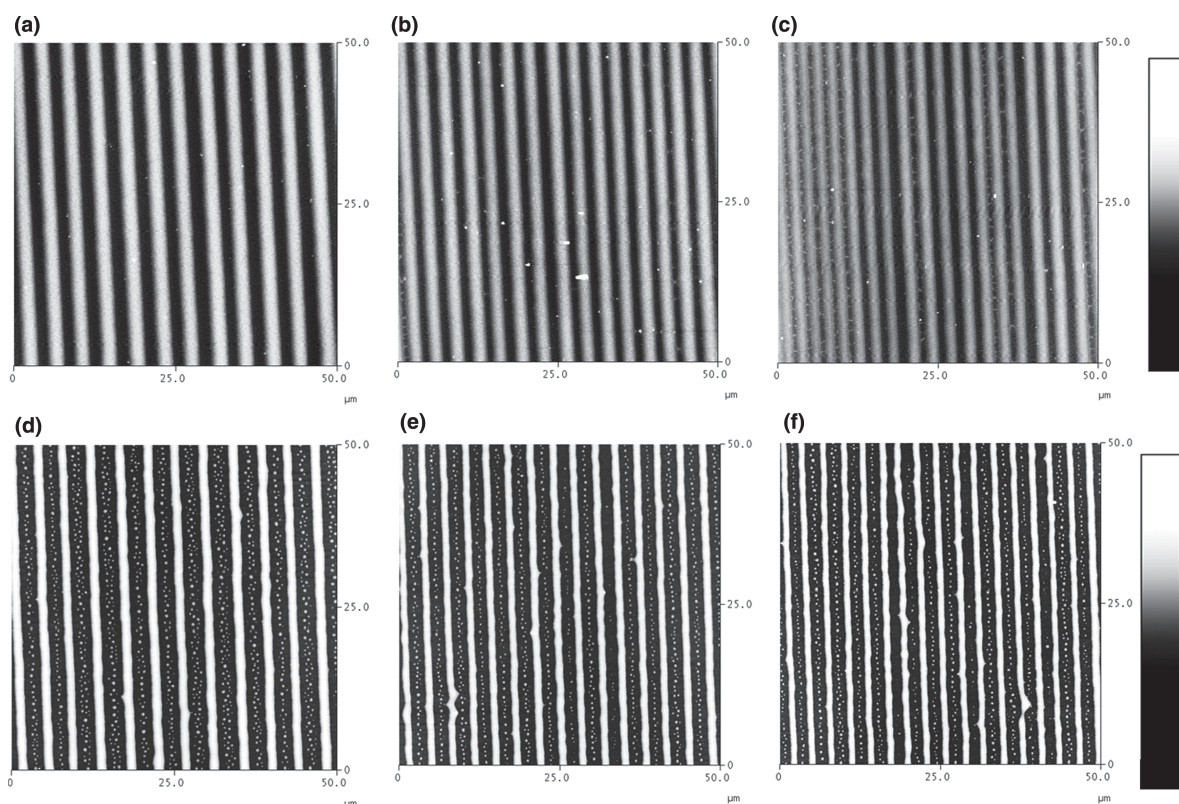


**Figure 3.** a–c) Representative AFM phase images of as-prepared CBCP stripes. As the contact line moved toward the wedge/Si contact center, the distance between adjacent stripes, the height of stripes, and the width of stripes, gradually decreased at the three regions. a) Outermost region ( $X_1$ ), b) intermediate region ( $X_3$ ), and c) innermost region ( $X_5$ ). d–f) Corresponding height images of CBCP stripes after THF vapor annealing for 10 h. Scan size = 50  $\mu\text{m} \times 50 \mu\text{m}$ .

Close examination of stripes revealed different degrees of microphase separation of CBCP within the microscopic stripes (2D AFM phase images; **Figure 4a, c, e, g, and i**, obtained right after evaporative self-assembly of CBCP in the wedge-on-Si geometry). Specifically, within a stripe, a disordered, nearly featureless morphology was observed next to the beginning of a contact line (i.e., the right side of the stripe, marked in Figure 4a, c, e, g, and i), while partially ordered nanodomains (i.e., in-plane cylindrical nanodomains, which appear dark; B blocks formed nanocylinders in the matrix of A and C blocks) were seen near the end of contact line (i.e., the left side of the stripe; Figure 4a, c, e, g, and i). The formation of such morphology can be rationalized as follows. In the area near the beginning of a contact line, the evaporation rate of toluene was considerably higher, leading to faster depletion of toluene and thus nearly featureless topology. By contrast, in the area near the end of a contact line, residual toluene was trapped due to the lengthy pinning of the contact line, thereby imparting the polymer chain mobility, which in turn promoted the microphase separation of CBCP, forming nanocylinders that lay parallel to the plane of the stripe in order to reduce the number of cylinder ends. These observations were reminiscent of a previous study on evaporative organization of polystyrene/poly(methyl methacrylate) (PS/PMMA) blend rings, where the residual solvent played an important role in forming topographic modulations on the ring surfaces in the late stage of phase segregation.<sup>[27]</sup>

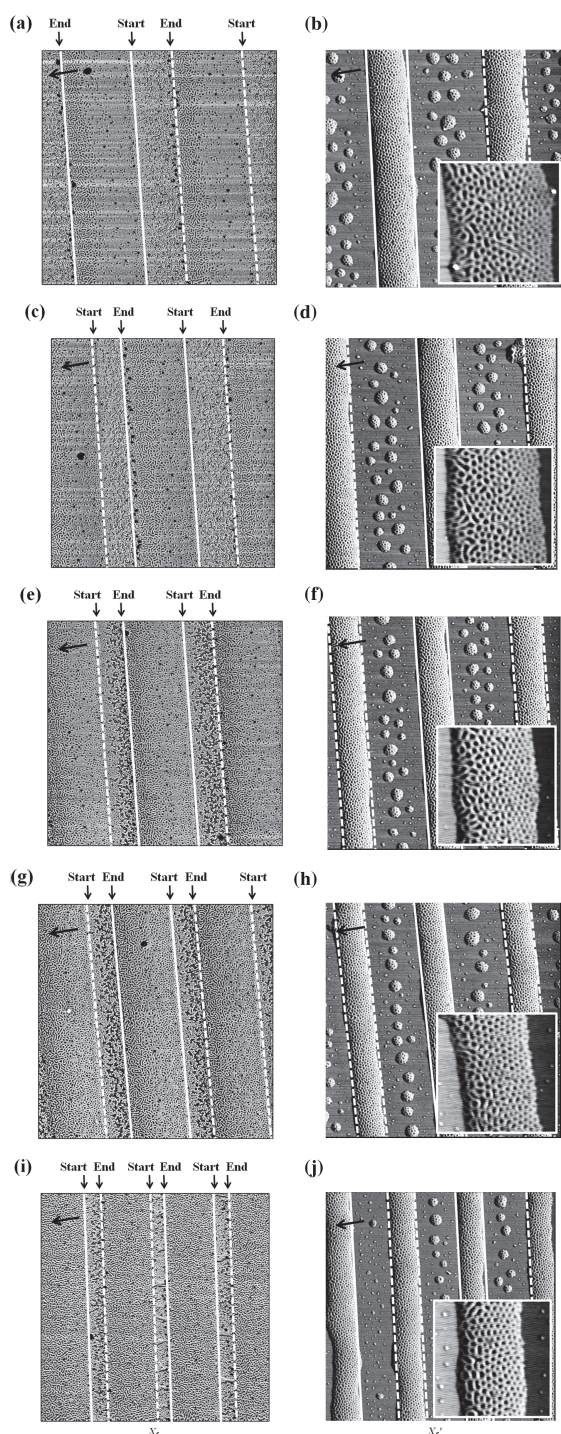


**Figure 4.** Morphological evolution of CBCP nanostructures within microscopic stripes during the course of THF vapor annealing. AFM phase images of self-assembled nanodomains obtained at five regions before (a at  $X_1$ , c at  $X_2$ , e at  $X_3$ , g at  $X_4$ , and i at  $X_5$ ) and after (b at  $X_1$ , d at  $X_2$ , f at  $X_3$ , h at  $X_4$ , and j at  $X_5$ ) THF vapor annealing. The transition from disordered (area near the end of contact line; labeled “End”) and in-plane nanocylinders (area near the beginning of contact line; labeled “Start”), connected by a monolayer of CBCP (i.e., interstripe regions, between the end of the previous contact line and the start of next contact line) (a, c, e, g, and i), to vertically oriented nanocylinders was observed after solvent vapor annealing (b, d, f, h, and j). The width of stripes before and after vapor annealing are marked with lines. Scan size =  $10 \mu\text{m} \times 10 \mu\text{m}$  and  $2 \mu\text{m} \times 2 \mu\text{m}$  (insets). Arrows indicate the direction that the contact line was moving.

The mixed morphology of disordered and partially ordered nanodomains (Figure 4a, c, e, g, and i (phase) and Supporting Information, Figure S1 (height)) was transformed into vertically oriented nanocylinders after exposure to saturated THF vapor (Figure 4b, d, f, h, and j and Supporting Information, Figure S1), thereby yielding hierarchically ordered structures; namely, gradient concentric rectangles were formed globally at the micrometer scale by controlled evaporative self-assembly of CBCP, and vertically aligned nanocylinders were formed at the nanometer scale within microscopic stripes by spontaneous self-assembly of CBCP that was promoted by the solvent vapor annealing. The cylindrical nanodomains were composed of B block and appeared dark in phase images (Figure 4) and lower in height images (Figure S1, Supporting Information); this is due to the presence of  $-C-O-C-$  in the B block, which makes it softer than C block, and the preferential swelling of the B block by THF vapor, followed by its contraction upon the evaporation of THF. The number of confined nanocylinders decreased as the width of a stripe decreased (i.e., from  $X_1$  to  $X_5$ ; insets in Figure 4b, d, f, h, and j).

Comparing the images of as-prepared samples (Figure 3a–c and Figure 4a, c, e, g, and i) with those after vapor annealing (Figure 3d–f and Figure 4b, d, f, h, and j), a very thin monolayer of CBCP molecules, exhibiting cellular morphology that resembles randomly distributed surface undulations occurring in the early stage of dewetting,<sup>[28]</sup> was formed in the area between adjacent stripes before the solvent annealing. This can be attributed to the favorable interaction of hydrophilic groups of the polymer backbone with the native silicon oxide on the Si substrate during the “slip” process of the three phase contact line. Upon exposure to THF vapor, the hydrophobic PS block dewetted from the Si substrate and formed circular shaped dots (i.e., solvent-driven dewetting<sup>[29]</sup>) in the central region between adjacent stripes (Figure 3d–f and Figure 4b, d, f, h, and j). Notably, the cylindrical nanodomains confined within these circular dots are clearly evident and they will be the subject of future study. It is interesting to note that similar deposits (i.e., the existence of thin layers between patterns) were observed in the study of hierarchically ordered poly(styrene-*b*-methyl methacrylate) (PS-*b*-PMMA) diblock copolymer thin films produced by other evaporative assembly methods.<sup>[30]</sup>

The mobility of CBCP was dramatically enhanced when exposed to THF vapor. The THF annealing provided the polymer backbone (A and B blocks) of CBCP stripes with slightly higher mobility due to the similarity in chemical structure between THF and the backbone. As a result, the polymer backbone was pulled from the Si/polymer interface to the polymer/air interface to contact preferentially with THF vapor. During the course of vapor annealing, the volume of polystyrene arms (i.e., C block) on the hydrophilic Si substrate increased. The stripes were thus easily shrunk, as hydrophobic polystyrene arms dewetted the hydrophilic Si substrate, i.e., they possessed a positive Hamaker constant.<sup>[10,28]</sup> Consequently, the stripes that were a few micrometers wide narrowed laterally while the average height of the stripes increased (Figure 3d–f and Figure 4b, d, f, h, and j) by approximately two times, compared to the sample prior to

the vapor annealing (Figure 3a–c and Figure 4a, c, e, g, and i). Representative changes in width and height at  $X_1$ ,  $X_3$ , and  $X_5$  are shown in Figure S2, Supporting Information; they are very flat ring-like stripes.

It is worth noting that such hierarchically structured block copolymer patterns can be controllably created, eliminating the need for the use of topographically or chemically patterned substrates prepared by costly multistep lithography techniques,<sup>[31,32]</sup> external fields, or additional surface neutralization by using a random copolymer brush to provide identical interfacial tension for each block to achieve vertically oriented nanostructures.<sup>[30]</sup> We note that the cylindrical nanodomains in the stripe were less ordered than those of a spin-coated film. This is presumably due to the thickness-modulated stripes formed by the evaporative self-assembly process (Figure 4) and the effect of residual solvent, which is trapped for a longer time near the end of the contact line (i.e., the left side of the stripe; Figure 4) than near the beginning of the contact line (i.e., the right side of the stripe; Figure 4), on the microphase separation of CBCP in the early stage, resulting in larger nanocylinders on the left than on the right. Based on AFM measurements, the characteristic distance between neighboring cylinders,  $L_0$ , and the average size of nanodomains,  $D$ , were  $125 \text{ nm} \pm 5 \text{ nm}$  and  $85 \text{ nm} \pm 5 \text{ nm}$ , respectively, corresponding to the values of  $L_0 = 130 \text{ nm} \pm 10 \text{ nm}$  and  $D = 87 \text{ nm} \pm 12 \text{ nm}$  in bulk.<sup>[24,25]</sup>

In summary, we have demonstrated a simple, robust means to create hierarchically ordered CBCP patterns by combining controlled evaporative self-assembly of capillary-held CBCP solution in the wedge-on-Si geometry, which yielded microscopic concentric gradient rectangles with spontaneous self-assembly of CBCP nanodomains that was facilitated by subsequent solvent vapor annealing. These highly ordered structures have potential applications in electronics, optics, and nanotechnology, and serve as a useful platform to study cell motility and adhesion, neuron guidance, and other processes involved in biological pattern formation and recognition. We envision that by varying the capillary height between the upper and lower surfaces of the confined geometry, the evaporative flux can be delicately tuned, and thus a family of diverse, intriguing surface patterns can be achieved. Moreover, by utilizing other self-assembling materials as building blocks, this facile, scalable approach may open a new avenue to create periodically well-defined, functional, self-assembled materials and versatile devices with hierarchical ordering of nanodomains for photonic, electronic, optoelectronic, and bioengineering applications, eliminating the need for physical or chemical templates, lithography techniques, and external fields.

## Experimental Section

**Synthesis and characterization of asymmetric comb block copolymer (CBCP):** A CBCP with an ultrahigh molecular weight was selected for use from a series of CBCPs synthesized in previous studies.<sup>[24,25]</sup> The molecular weight (MW) and polydispersity (PDI) were measured by size exclusion chromatography (SEC) on a machine equipped with refractive index and light scattering

detectors. The total MW of CBCP, composition ratio of the blocks, and PDI were  $510 \text{ kg mol}^{-1}$ , A : B : C = 100 : 1000 : 3740, and 1.08, respectively. The mol %/v fraction ratio of the blocks was A : B : C = 2/0.05 : 21/0.41 : 77/0.54. The asymmetric CBCP was dissolved in toluene to prepare the CBCP toluene solution at a concentration of  $0.25 \text{ mg mL}^{-1}$ . Subsequent purification of the solution was conducted using  $0.2 \mu\text{m}$  hydrophobic membrane filters.

**Wedge-on-flat geometry:** A wedge lens made of aluminum and a Si wafer were used as the upper and lower surfaces, respectively, to construct a confined geometry, i.e., the wedge-on-flat geometry. The area of the sides of the wedge,  $A$ , and the wedge height,  $H$ , were  $1 \text{ cm} \times 1 \text{ cm}$  and  $1000 \mu\text{m}$ , respectively. The Si substrates were cleaned using a mixture of sulfuric acid and NOCHROMIX. They were vigorously rinsed with DI water and blown dry with  $\text{N}_2$ . The contact of the wedge with Si in a sealed chamber was made using a computer-programmable inchworm motor with a step motion at the micrometer scale. The wedge-on-flat geometry was placed in a sealed chamber to minimize possible air convection and to maintain constant temperature during the evaporation process. The loading of the CBCP toluene solution in the wedge-on-flat geometry resulted in a liquid capillary bridge with the highest evaporation rate at the edge of the capillary (Figure 1c).

**Solvent vapor induced surface reconstruction:** The surface patterns of CBCP formed on the Si substrate were exposed to THF vapor for 10 h in a sealed Teflon vessel to promote microphase separation of CBCP. The volume of the vessel was  $29.4 \text{ cm}^3$  and a small piece of gauze soaked with  $10 \mu\text{L}$  of THF was placed on the bottom.

**Evaluation of CBCP surface morphologies:** The evaporation typically took 30 min to complete, after which the wedge and Si substrate were separated. Due to the inclination of wedge, only the patterns formed on flat Si substrate were thoroughly examined by optical microscopy (BX51 optical microscope (Olympus) in reflection mode) and AFM (Dimension 3100 scanning force microscope in tapping mode (Digital Instrument)). BS-tap300 tips (Budget Sensors) with spring constants ranging from 20 to  $75 \text{ N m}^{-1}$  were used as scanning probes. The surface patterns were re-examined at identical positions,  $X_n$  ( $n = 1-5$ ) from the same sample, ensuring rational comparisons of surface morphologies before and after THF vapor annealing.

## Supporting Information

Supporting information is available from the Wiley Online Library or from the author.

## Acknowledgements

We gratefully acknowledge support from the National Science Foundation (NSF CAREER Award, CBET-0844084) and the Key Laboratory of Molecular Engineering of Polymers at Fudan University (Ministry of Education, China). We also thank Q. Zou for AFM use.

- [1] H. O. Jacobs, A. R. Tao, A. Schwartz, D. H. Gracias, G. M. Whitesides, *Science* **2002**, *296*, 323.
- [2] B. P. Khanal, E. R. Zubarev, *Angew. Chem., Int. Ed.* **2007**, *46*, 2195.
- [3] R. D. Deegan, O. Bakajin, T. F. Dupont, G. Huber, S. R. Nagel, T. A. Witten, *Nature* **1997**, *389*, 827.
- [4] E. Pauliac-Vaujour, A. Stannard, C. P. Martin, M. O. Blunt, I. Notingher, P. J. Moriarty, I. Vancea, U. Thiele, *Phys. Rev. Lett.* **2008**, *100*, 176102.
- [5] D. J. Harris, H. Hu, J. C. Conrad, J. A. Lewis, *Phys. Rev. Lett.* **2007**, *98*, 148301.
- [6] H. Yabu, M. Shimomura, *Adv. Funct. Mater.* **2005**, *15*, 575.
- [7] S. W. Hong, S. Giri, V. S. Y. Lin, Z. Q. Lin, *Chem. Mater.* **2006**, *18*, 5164.
- [8] S. W. Hong, W. Jeong, H. Ko, M. R. Kessler, V. Tsukruk, Z. Q. Lin, *Adv. Funct. Mater.* **2008**, *18*, 2114.
- [9] S. W. Hong, J. Xia, M. Byun, Q. Zou, Z. Q. Lin, *Macromolecules* **2007**, *40*, 2831.
- [10] S. W. Hong, J. Xia, Z. Q. Lin, *Adv. Mater.* **2007**, *19*, 1413.
- [11] S. W. Hong, J. Xu, Z. Q. Lin, *Nano Lett.* **2006**, *6*, 2949.
- [12] S. W. Hong, J. Xu, J. Xia, Z. Q. Lin, F. Qiu, Y. L. Yang, *Chem. Mater.* **2005**, *17*, 6223.
- [13] M. Gleiche, L. F. Chi, H. Fuchs, *Nature* **2000**, *403*, 173.
- [14] X. Chen, A. L. Rogach, D. V. Talapin, H. Fuchs, L. F. Chi, *J. Am. Chem. Soc.* **2006**, *128*, 9592.
- [15] B. G. Prevo, O. D. Velev, *Langmuir* **2004**, *20*, 2099.
- [16] S. W. Hong, M. Byun, Z. Q. Lin, *Angew. Chem., Int. Ed.* **2009**, *48*, 512.
- [17] J. Xu, J. Xia, S. W. Hong, Z. Q. Lin, F. Qiu, Y. L. Yang, *Phys. Rev. Lett.* **2006**, *96*, 066104.
- [18] J. Xu, J. Xia, Z. Q. Lin, *Angew. Chem., Int. Ed.* **2007**, *46*, 1860.
- [19] S. W. Hong, J. Wang, Z. Q. Lin, *Angew. Chem., Int. Ed.* **2009**, *48*, 8356.
- [20] M. Maldovan, E. L. Thomas, *Nat. Mater.* **2004**, *3*, 593.
- [21] Y. Lin, A. Boker, J. He, K. Sill, H. Xiang, C. Abetz, X. Li, J. Wang, T. Emrick, S. Long, Q. Wang, A. Balazs, T. P. Russell, *Nature* **2005**, *434*, 55.
- [22] K. L. Genson, J. Hoffman, J. Teng, E. R. Zubarev, D. Vaknin, V. V. Tsukruk, *Langmuir* **2004**, *20*, 9044.
- [23] K. L. Genson, J. Holzmueller, C. Y. Jiang, J. Xu, J. D. Gibson, E. R. Zubarev, V. V. Tsukruk, *Langmuir* **2006**, *22*, 7011.
- [24] M. B. Runge, N. B. Bowden, *J. Am. Chem. Soc.* **2007**, *129*, 10551.
- [25] M. B. Runge, C. E. Lipscomb, L. R. Ditzler, M. K. Mahanthappa, A. V. Tivanski, N. B. Bowden, *Macromolecules* **2008**, *41*, 7687.
- [26] L. Zhao, M. D. Goodman, N. B. Bowden, Z. Q. Lin, *Soft Matter* **2009**, *5*, 4698.
- [27] M. Byun, S. W. Hong, F. Qiu, Q. Zou, Z. Lin, *Macromolecules* **2008**, *41*, 9312.
- [28] R. Xie, A. Karim, J. F. Douglas, C. C. Han, R. A. Weiss, *Phys. Rev. Lett.* **1998**, *81*, 1251.
- [29] S. H. Lee, P. J. Yoo, S. J. Kwon, H. H. Lee, *J. Chem. Phys.* **2004**, *121*, 4326.
- [30] B. H. Kim, D. O. Shin, S.-J. Jeong, C. M. Koo, S. C. Jeon, W. J. Hwang, S. Lee, M. G. Lee, S. O. Kim, *Adv. Mater.* **2008**, *20*, 2303.
- [31] R. A. Segalman, H. Yokoyama, E. J. Kramer, *Adv. Mater.* **2001**, *13*, 1152.
- [32] S. O. Kim, H. H. Solak, M. P. Stoykovich, N. J. Ferrier, J. J. de Pablo, P. F. Nealey, *Nature* **2003**, *424*, 411.

Received: May 12, 2010  
Published online: September 3, 2010